JOURNAL OF CATALYSIS **161,** 143–155 (1996)
ARTICLE NO. 0171

Ethylene Oxidation on Polycrystalline Platinum over Eight Orders of Magnitude in Ethylene Pressure: A Kinetic Study in the Viscous Pressure Regime

U. Ackelid, L. Olsson, and L.-G. Petersson

Laboratory of Applied Physics, Department of Physics and Measurement Technology, Linköping University, S-581 83 Linköping, Sweden

Received April 17, 1995; revised December 7, 1995; accepted February 2, 1996

C_2H_4 oxidation on polycrystalline Pt films and foils at $T = 373$–473 K was studied with mass spectrometry in the pressure ranges 10^{-6}–10^2 Torr C_2H_4 and 0.3–1500 Torr O_2 (1 Torr = 133.3 Pa). A new, "spatially resolved gas sampling" method enabled true kinetic data to be collected in the viscous pressure regime. *In situ* measurements of surface hydrogen with a capacitance–voltage technique and *ex situ* characterization with Auger electron spectroscopy and atomic force microscopy were also performed. No structure sensitivity with respect to sample grain size could be seen. The reaction orders in C_2H_4 and O_2 were +1 and −1 in oxygen excess, −2 and +3 in weak ethylene excess, and −0.5 and +1 in large ethylene excess, respectively. The apparent activation energy was between 30 and 75 kJ/mol for different reactant mixtures. The rate data could be qualitatively fitted to a simple Langmuir–Hinshelwood reaction scheme in the excess regimes, assuming competitive adsorption of C_2H_4 and O_2, abundant molecular desorption of the excess reactant, and a strong self-inhibition of C_2H_4 adsorption.

INTRODUCTION

Oxidation of hydrocarbons over platinum is one of the key processes in car exhaust conversion, and that is an obvious motive for studies of such reactions. Ethylene is a suitable test gas for several reasons: it is a fairly simple hydrocarbon, it interacts with metal surfaces even at moderate temperatures, and it gives few possible oxidation products. There are numerous investigations of ethylene interaction with clean (1–10) and oxygen-covered (8–10) Pt surfaces in ultrahigh vacuum (UHV) and also many studies of the $C_2H_4 + O_2$ reaction near 1 atm (11–29). However, most of the latter have been done with supported Pt catalysts (12–16, 18, 21–24, 26) or with porous Pt films (17, 19, 20, 25); literature data on macroscopic Pt surfaces are scarce (11, 27–29).

Table 1 presents data from isothermal kinetic studies at near-atmospheric pressures published throughout the past three decades. CO_2 and H_2O are the chief reaction products in all cases and partially oxidized species are explicitly reported only once (12). Positive first reaction order in ethylene in fuel-lean mixtures is also unanimously reported, but the order in ethylene excess and the dependence on oxygen pressure are not yet agreed upon. Both Rideal–Eley (R–E) and Langmuir–Hinshelwood (L–H) reaction mechanisms have been suggested. Two other interesting observations in Table 1 are the scatter of the activation energies and the vary narrow pressure ranges (maximum two orders of magnitude) used in all previous studies.

There are also studies using other approaches than the "rate vs pressure at constant temperature" concept. Wolf *et al.* (21) used temperature and concentration programming techniques, FTIR spectroscopy, and computer simulations to investigate the $C_2H_4 + O_2$ reaction over supported Pt/SiO_2. Their results indicate that the reaction is of L–H type, but that the reaction pathways under fuel-lean and fuel-rich conditions differ significantly. In addition, this group have investigated self-sustained rate oscillations (22–24), previously observed by others (15, 17, 25). Sheintuch *et al.* performed nonisothermal experiments with Pt/Al_2O_3 (26) and Pt wires (27), which also indicate a L–H rate expression. Kunimori *et al.* (28) detected syngas production ($CO + H_2$) in molecular beam experiments with a Pt foil at higher temperatures (>700 K) and lower pressures ($\approx 10^{-2}$ Torr). Wu and Phillips (29) found that the $C_2H_4 + O_2$ reaction on Pt may induce catalytic etching and deposition of carbon; however, these phenomena were never seen at temperatures below 770 K.

Despite the work done in the past, there are still lacking fundamental data for the $C_2H_4 + O_2$ reaction on macroscopic Pt surfaces and, consequently, macroscopic and supported systems have never been systematically compared. A flat, continuous surface has some experimental advantages over a supported catalyst: it is easily examined by surface-sensitive techniques, it is often less prone to reconstruction, its surface area and temperature are easily determined, and its catalytic action is solely controlled by the metal properties.

This communication describes a study of ethylene oxidation over various polycrystalline platinum surfaces. In

0021-9517/96 $18.00

TABLE 1

Collection of Kinetic Data from Isothermal Studies of C_2H_4 Oxidation on Pt at Near-Atmospheric Pressures

Ref.	Catalyst	Pressure (Torr)		T (K)	Orders		E^a (kJ/mol, apparent)	Comments
		C_2H_4	O_2		C_2H_4	O_2		
11	Evaporated Pt film	2.3	24	280–370	ns	ns	49	Static reactor study
12	Pt/SiO_2 (dispersed)	3–80	10–150	350–380	−1	+1	77	Traces of acetic acid and acetaldehyde
13–14	Pt/Al_2O_3 (dispersed)	1–20	150	390	+1 (low p) −1 (high p)	ns	ns	Structure sensitivity observed
15	Pt/Al_2O_3 (dispersed)	0.5–20	3–150	360–470	−1	+1	102	Oscillations observed
16	Pt/Al_2O_3 (dispersed)	ns	ns	ns	+1 (low p) −1 (high p)	ns	31 91	L–H rate eq. proposed
17	Porous Pt film on ZrO_2	3–15	5–30	470–670	+1 (low p) 0 (high p)	0 +1	25 70	R–E model, oscillations observed
18	Pt/Al_2O_3 (dispersed)	0.1–3	6–40	340–360	+1 (low p) −1 (high p)	−1 +1	108 77	L–H rate eq. proposed
19	Porous Pt film on ZrO_2	ns	ns	570–720	+1 (low p) 0 (high p)	0 +1	46–109 8–25	R–E model
20	Porous Pt film on Al_2O_3	0.04–4	4–110	420–560	+1 (low p) 0? (high p)	0 +1	78 ns	R–E/L–H model
This study	Dense Pt film on SiO_2 and Pt foil	10^{-6}–10^2	0.3–1500	373–473	+1 (low p) −2 (med. p) −0.5 (high p)	−1 +3 +1	See Fig. 11	

Note. ns, not specified.

a forthcoming paper (30), the work will be extended to planar, supported model catalysts. The aim is, besides extending the present knowledge of the reaction kinetics, to sort out phenomena related to the metal itself, to the structure, and to the support. We have expanded the pressure ranges considerably in comparison with previous studies; C_2H_4 and O_2 pressures have been varied over eight and four orders of magnitude, respectively. A recently developed experimental technique, spatially resolved gas sampling (SRGS) (31–34), has been employed to follow the reaction at high pressures, where mass-transport limitations would make conventional methods ill-defined. Our samples are made by Pt evaporation onto oxidized silicon substrates. Thus various structures can be fabricated, from dense films down to small, well-separated Pt islands surrounded by SiO_2, simply by varying the amount of evaporated metal. The focus of this paper is on dense Pt films and also, for comparison, a Pt foil.

EXPERIMENTAL DETAILS

Equipment and Materials

The platinum samples were all polycrystalline and consisted of a foil and several evaporated films. The foil was supplied by Goodfellow Metals Ltd. and was of high purity (99.99+%). It was 0.1 mm thick and had an area of 11×17 mm^2. Prior to first use, it was subjected to conventional washing procedures for UHV components.

The Pt film samples were fabricated according to a standard procedure (35), involving thermal growth of 100 nm amorphous SiO_2 on 0.4 mm thick, polished silicon wafers followed by electron-gun evaporation of 100 nm Pt in a UHV chamber. The evaporation was performed with room-tempered substrates, which results in a dense Pt layer dominated by small grains (36). Since the substrate is amorphous, it should not induce any preferential direction of the Pt crystal growth. It can be shown by thermodynamic arguments that the Pt (111) surface has the lowest free energy (1); thus it is reasonable to assume that many of the grains are oriented in the (111) direction. The film samples were cut into 14×14 mm^2 pieces but otherwise used as received from the evaporation chamber.

A separate Auger electron spectroscopy (AES) system was used for surface analysis of fresh samples and of samples subjected to several reaction studies. Figure 1 shows two representative AE spectra. Ca, Fe, S, Cl, and O, elements which are not uncommon on nominally pure Pt (37–40), were clearly detected on the unused foil (spectrum (b)) and also, in smaller amounts, on the used foil. Furthermore,

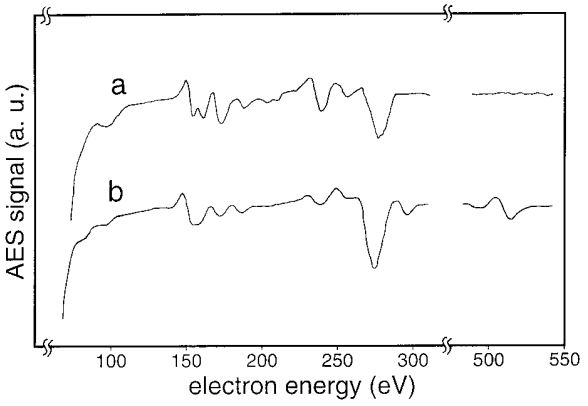

FIG. 1. Auger electron spectra of unsputtered Pt samples. (a) A used Pt film. (b) The unused Pt foil. The carbon signals at 275 eV have an intensity typical of any unsputtered sample analyzed in our AES instrument; they are attributed to some contamination source in the sample transfer procedure. Spectrum (b) indicates presence of a large amount of SiO_x (80 eV), S (155 eV), Cl (180 eV), Ca (295 eV), O (515 eV), and Fe (600, 650, 705 eV, not shown). Spectrum (a) resembles a clean Pt spectrum, except for the carbon peak. In particular, SiO_x is not seen in spectrum (a). All contaminants could be removed by Ar sputtering.

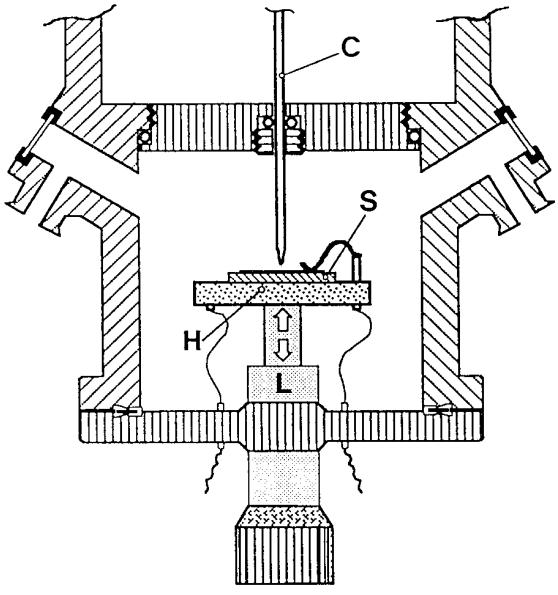

FIG. 2. The microreactor used in this study. S, Pt sample (foil or film); H, heated sample holder; C, quartz capillary; L, linear transfer mechanism.

a shoulder was observed on the Pt (64 eV) AES peak, probably indicating a SiO_x contamination (37, 38). The carbon peak at 275 eV is attributed to some contamination process taking place during the transfer of the sample into the AES instrument.

The films appeared much cleaner than the foil (see spectrum (a) in Fig. 1). Ca and Fe were never seen, but the "SiO_x shoulder" and an accompanying O(510 eV) peak were discernible in a few cases for unused as well as used films. We believe that this is due to a substrate SiO_2 contribution through occasional cracks in some films rather than SiO_x segregation on top of the films; otherwise the SiO_x shoulder should have been a regular feature in the AE spectra. In conclusion, the foil and all the films give very similar and reproducible results in the rate measurements presented below. This suggests that there is little influence of contaminants or that the reaction rates of all samples, despite the various levels of contamination indicated by AES, are influenced to a very similar extent.

Atomic force microscopy (AFM) was used for characterization of the surface topography of some samples (see Figs. 7a–7c). The images were obtained with a separate, commercial instrument (Nanoscope III by Digital Instruments) operated in "tapping mode."

The apparatus for reaction studies has been described in detail in preceding publications (31, 34). In brief, it consists of a microreactor and a gas analysis system based on mass spectrometry. The microreactor, schematically shown in Fig. 2, has a volume of about 100 ml. A planar catalyst sample (S) is mounted on a ceramic sample holder (H), which is heated by a built-in heating resistor. The sample temperature is measured by a Pt resistor placed underneath, and touching, the sample. In all experiments described here, temperatures were in the range 373–473 K. The microreactor and parts of the gas inlet system can be heated by an external jacket and they were kept at a temperature about 10 K lower than the sample. Figure 2 also shows a quartz capillary (C) (34, 41), which serves as a gas leak into a quadrupole mass spectrometer. The gas consumption of the capillary is negligible, due to a narrow restriction at the capillary tip (34, 41). The sample holder can be moved along the capillary axis by means of a linear transfer mechanism (L), and thus it is possible to measure partial gas concentrations as a function of distance from the catalyst. This forms the basis of the SRGS technique described below.

The microreactor is run in a continuous-flow mode and supplied with gas by a number of mass-flow controllers. The gases in this study, oxygen (99.998%), ethylene (99.95%), argon (99.9997%), hydrogen (99.9996%), and carbon dioxide (99.998%), were used without further purification. Argon served as a carrier gas for the main reactants O_2 and C_2H_4, H_2 was used for sample treatments, and CO_2 for pressure calibration. The total gas flow through the microreactor was about 700 ml_n/min in all experiments. Four different O_2 pressures (0.3, 3, 150, and 1500 Torr) were used and the nominal C_2H_4 pressure was in the range 10^{-4}–100 Torr. The C_2H_4 pressure close to the catalyst surface (sampled by the capillary leak) could, however, be as low as 10^{-6} Torr under reaction conditions.

The film samples also function as hydrogen-sensitive metal–insulator–semiconductor (MIS) capacitors (35). A schematic MIS capacitor and its capacitance–voltage (C–V)

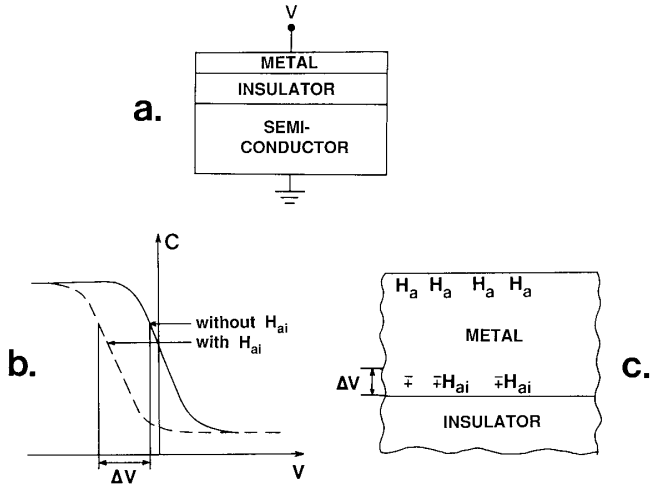

FIG. 3. (a) A schematic metal– insulator–semiconductor (MIS) capacitor. (b) Capacitance–voltage curves of a MIS capacitor with and without hydrogen (H_{ai}) at the metal–insulator interface. ΔV is the "C–V signal." (c) The detection mechanism. Hydrogen (H_a) on the metal surface diffuses through the metal into the metal–insulator interface. The C–V signal (ΔV) is caused by a polarization of the hydrogen atoms (H_{ai}) at the interface.

characteristics are shown in Figs. 3a and 3b. The hydrogen-sensing mechanism is based on the fact that hydrogen atoms may penetrate through metals like Pt and Pd. Hydrogen atoms, adsorbed on the metal surface (H_a in Fig. 3c), diffuse to and adsorb at the metal–insulator interface (H_{ai}). The interface hydrogen lowers the metal work function, which can be observed as a voltage shift of the C–V curve (ΔV in Fig. 3b). The hydrogen diffusion is reversible; thus ΔV (or the "C–V signal") is a function of the coverage of free hydrogen atoms on the metal surface under steady-state conditions. Hydrogen sensing with MIS capacitors is reviewed elsewhere (35).

The C–V curve of an MIS capacitor can also be used for temperature measurements. The inversion capacitance, i.e., the rightmost part of the C–V curve in Fig. 3b, is very sensitive to temperature variations (42). This property was used to confirm that the temperature difference between the metal film and the back of the silicon substrate was always negligible ($\leq$1 K). Thus the sample and the sample holder formed an isothermal system.

Spatially Resolved Gas Sampling (SRGS)

Pressure gradients due to diffusion limitations is a classic problem in reaction studies in the viscous pressure regime (43). Recently, we suggested a new experimental technique, SRGS (31, 32, 34), which allows steady-state rate vs pressure measurements even in presence of gradients. The SRGS concept is simple: gas transport is assumed to be dominated by diffusion in the vicinity of a macroscopic catalytic surface, local pressures are measured as a function of distance from the surface, and reaction rates and surface pressures are finally calculated using elementary diffusion laws. If the surface is plane and the temperature (T) and diffusion coefficients (D) in the gas mixture are constant, then the pressure gradients are linear and global diffusion rates (J) are given by Fick's first law,

$$J = -\frac{D}{RT}\frac{dp}{dx}, \qquad [1]$$

where R is the universal gas constant. Furthermore, the linear gradients are easily extrapolated to zero distance, so that true surface pressures of reactants are obtained. The impingement rate of a reactant is then given by

$$F = \frac{p}{\sqrt{2\pi MRT}}, \qquad [2]$$

where p is the extrapolated pressure and M is the molar mass. The reaction probability of the reactant is finally obtained as the consumption rate (Eq. [1]) divided by the impingement rate (Eq. [2]):

$$r = \frac{J}{F}. \qquad [3]$$

In case the reactant adsorbs before reacting and molecular desorption of the reactant is negligible, this reaction probability will be equal to the sticking coefficient (32).

SRGS has previously been applied to the $H_2 + O_2$ reaction on Pt, and reaction rates calculated from Eq. [1] were in good agreement with rates determined by an independent method (32).

Initial tests indicated that SRGS is particularly simple to apply to the $C_2H_4 + O_2$/Pt reaction, because gradients were found only in C_2H_4 pressure and never in O_2 pressure. We could thus study various C_2H_4 pressures in a constant nominal O_2 pressure and no corrections were needed in order to keep the O_2 surface pressure constant. In addition, the most interesting features of the reaction appear at very low C_2H_4/O_2 ratios, where it is safe to assume a constant C_2H_4 diffusion coefficient. At the lowest O_2 pressures, however, we mixed the reactants with argon to keep $D_{C_2H_4}$ constant. Figure 4 shows typical pressure gradients of C_2H_4 and the reaction products CO_2 and H_2O. Excellent linearity was found at distances between 0.2 and 1.4 mm, except for the highest O_2 pressure (1500 Torr), where the linear region was reduced to 0.1–0.5 mm. Consumption rates and production rates were calculated using Eq. [1] with diffusion coefficients from Ref. 44, and the rates were always in very good stoichiometric agreement (Fig. 5). The extrapolated C_2H_4 surface pressure was found accurate (maximum error $\approx$20%) as long as it did not fall below 1% of the nominal pressure (34). Such extreme ethylene depletion was occasionally observed at low O_2 pressures and the corresponding, less accurate, data points are explicitly marked in the figures below. The reproducibility of our measurements is further discussed in next section (see also Fig. 6).

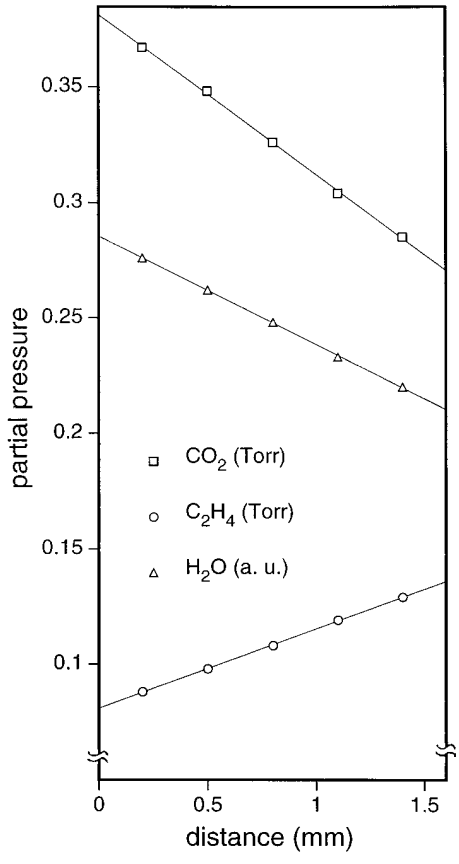

FIG. 4. Partial pressures of C_2H_4, CO_2, and H_2O measured with SRGS at various distances from a Pt film at $T = 423$ K. The nominal gas mixture contained 150-Torr O_2 and 0.33-Torr C_2H_4.

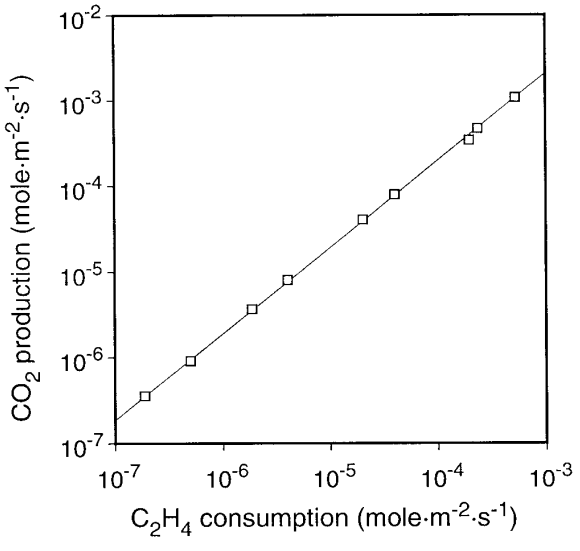

FIG. 5. CO_2 production rate vs C_2H_4 consumption rate for a Pt film at $T = 473$ K. The rates were calculated from partial pressure gradients using the SRGS evaluation method. The O_2 pressure was 150 Torr and the C_2H_4 pressure was varied over six decades ($\approx 10^{-5}$–10 Torr).

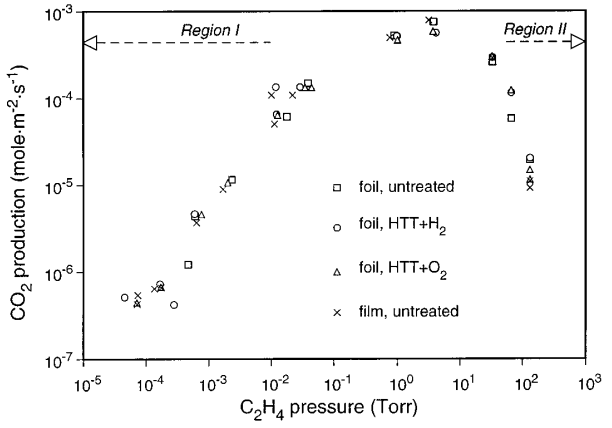

FIG. 6. CO_2 production rate vs C_2H_4 pressure at $T = 423$ K and 1500-Torr O_2 for a new, untreated Pt film (×), a new, untreated Pt foil (□), the Pt foil after a high-temperature treatment (HTT) with H_2 cooling (○), and the Pt foil after a HTT with O_2 cooling (△). The HTT consisted of 10 alternating, 1-min exposures to 150 Torr of O_2 and H_2, respectively, at a sample temperature of 623 K, followed by rapid cooling to 423 K in either 150-Torr H_2 or 150-Torr O_2. "Region I" and "Region II" define the regions of oxygen excess and ethylene excess, respectively.

In conclusion, we are convinced of the validity of the SRGS evaluation method.

SRGS thus provides true kinetic data even for diffusion-controlled reactions. Experimental difficulties may arise, however, in pressure regions where the rate derivative with respect to pressure is large and negative. A minute change of the nominal reactant pressure may then induce a giant leap of the surface pressure as the system switches between kinetic control and diffusion control (45). This phenomenon is discussed in detail elsewhere (34); it is, however, the reason for the lack of rate data near the rate maximum in some experiments presented below.

Reaction rates and impingement rates are given in units of mol m^{-2} s^{-1} throughout this paper. These have been calculated assuming a perfectly planar catalyst surface, and no corrections have been made for the microstructure of individual samples. Calculations based on the topography of AFM pictures (cf. Fig. 7) indicate that the correction factor would be only a few percent. Moreover, the calculated reaction probabilities (Eq. [3]) are, of course, independent of area corrections.

RESULTS AND DISCUSSION

General Observations and Structure Insensitivity

In accordance with most previous studies (11, 13–20), CO_2 and H_2O were the only detected products in all experiments. The mass spectrometer range 1–50 amu was investigated in detail for various C_2H_4/O_2 ratios, but partially oxidized products were never observed. The linearity in Fig. 5

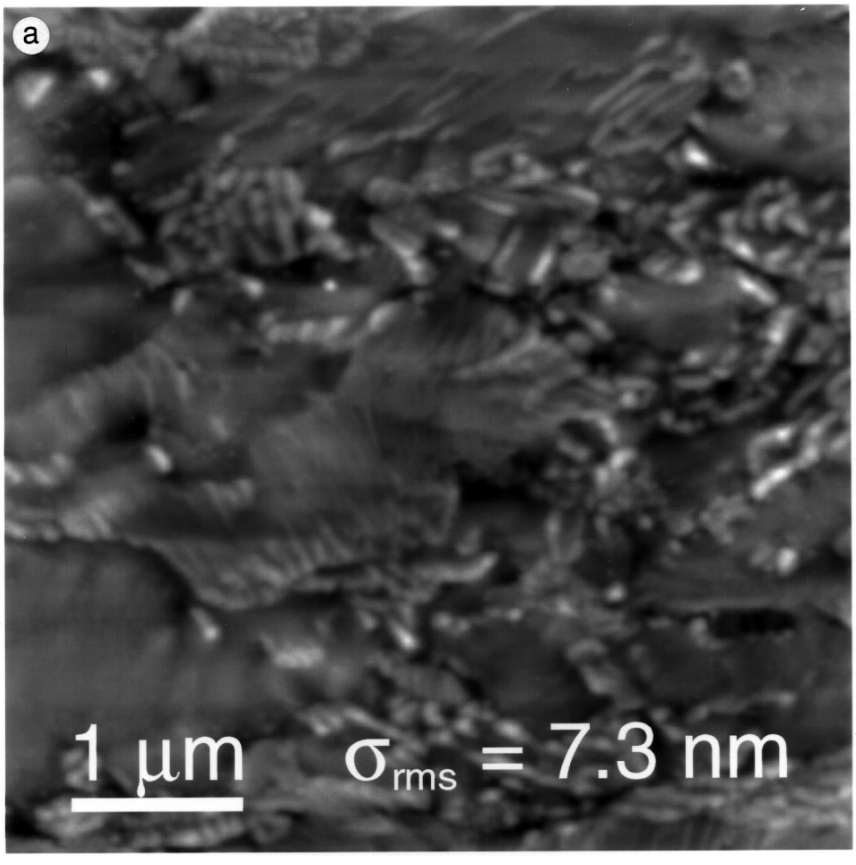

FIG. 7. Topography of Pt samples imaged by atomic force microscopy. (a) The Pt foil after a high-temperature treatment (HTT, see Fig. 6). (b) A Pt film after a HTT. (c) A Pt film never heated above 423 K. σ_{rms} is the root mean square of the surface roughness. The gray scale corresponds to a vertical height range of (a) 67 nm, (b) 22 nm, and (c) 9.3 nm. The surface area, as calculated from the topographical data, exceeds the nominal area by (a) 1.8%, (b) 1.4%, and (c) 2.9%.

further confirms that complete oxidation is the dominating reaction path. However, we cannot exclude that minute amounts (of the order of 1%) of CO could be formed, since the mass spectrum of CO interferes with that of CO_2. Furthermore, reaction rates were single-valued functions of reactant surface pressures and they remained reproducible over several weeks of reaction studies. Rate oscillations were never observed, neither on the foil nor on the films, in contrast to Refs. 15, 17 and 22–25. This may be due to different experimental conditions with respect to isothermality, mass transfer, or surface cleanliness.[1]

Figure 6 shows the reaction rate vs C_2H_4 pressure for the foil and a film at constant O_2 pressure (1500 Torr) and temperature (423 K). The reaction order in C_2H_4 is positive at low pressures (oxygen-dominated surface) and turns negative at higher pressures (ethylene-dominated surface), in line with previous studies on supported catalysts (13, 14, 16, 18). For brevity, these asymptotic regions on either side of the rate maximum will be referred to as "Region I" and "Region II," respectively. It is quite clear that these regions can be reached only if the C_2H_4 pressure is varied over several orders of magnitude. Figure 6 also shows that the foil and the film give practically identical rates over the entire C_2H_4 pressure range, and this was observed at all tested O_2 pressures. The rate curve of the foil is well reproduced even after repeated exposures to high H_2 and O_2 pressures at 673 K. The same was true for the film (not shown).

Figures 7a–7c show AFM images of the foil and a film that have been H_2/O_2-treated at 673 K and also a film that has been used for ethylene oxidation but never heated above 423 K. It is obvious that these three surfaces differ substantially with respect to microstructure. The large grains of the foil (Fig. 7a) and the grains of the untreated film (Fig. 7c) have sizes of the order of 1 μm and 10 nm, respectively, i.e., a difference of two orders of magnitude. Yet all samples yield identical rates of ethylene oxidation. We conclude that we have *no evidence for structure sensitivity for a macroscopic, polycrystalline Pt surface.* This observation can be compared with the ethylene hydrogenation reaction

[1] In an initial test prior to this study, we actually observed rate oscillations on a Pt film that had been inadvertently contaminated with molybdenum. However, we could never reproduce the oscillations on fresh samples after removal of the contamination source.

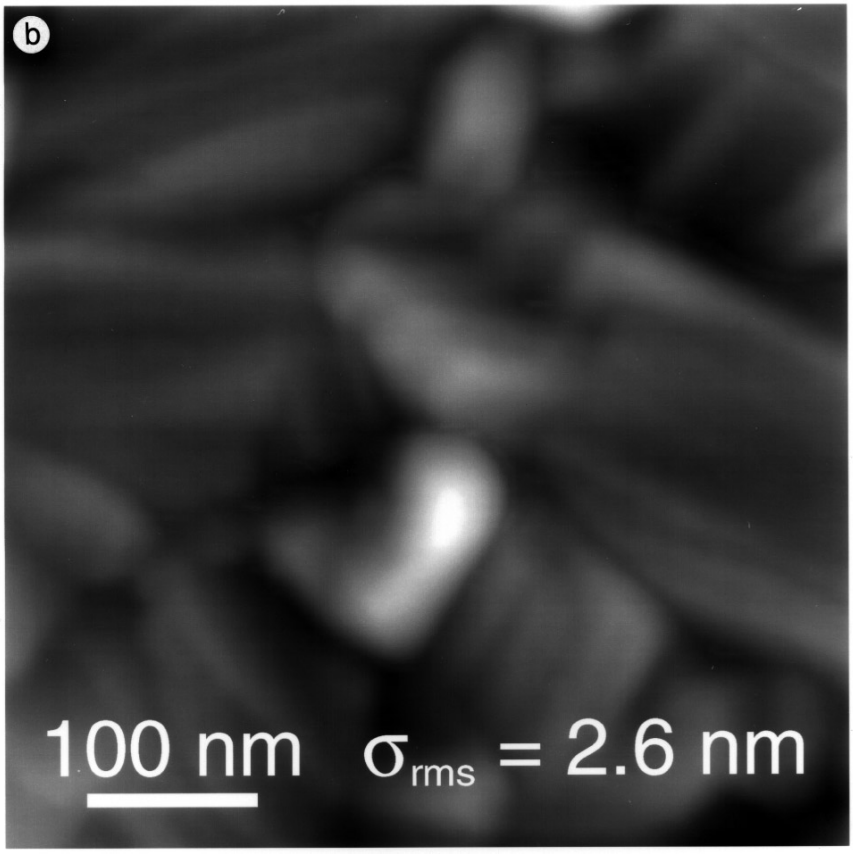

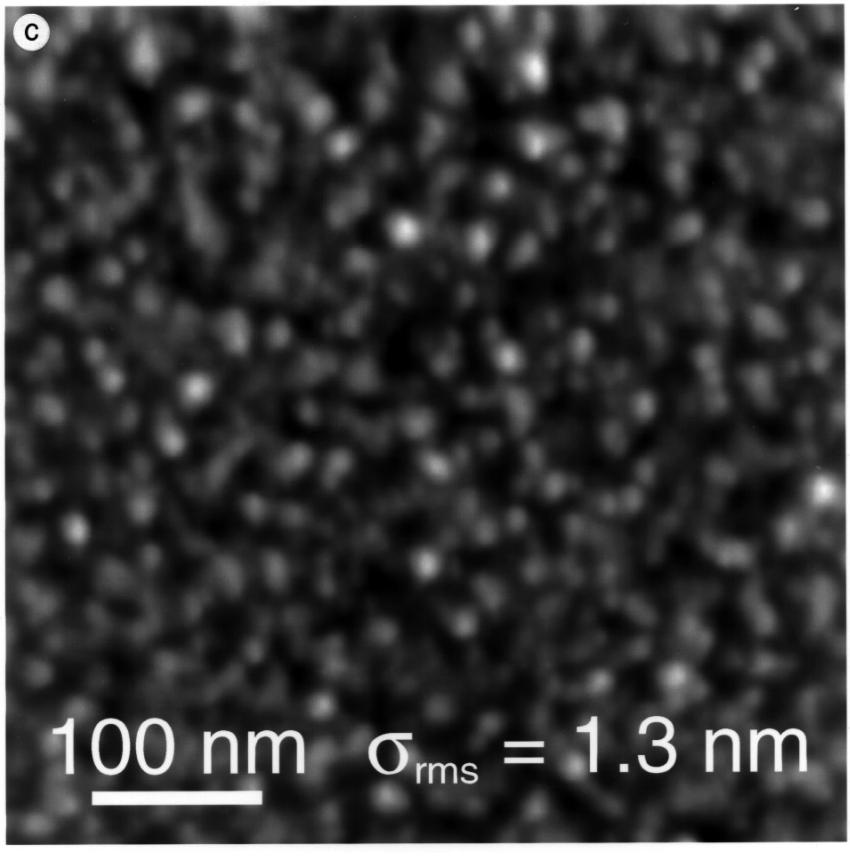

FIG. 7—*Continued*

over platinum (1, 46). The hydrogenation is thought to take place on top of a strongly adsorbed carbonaceous overlayer that screens the microstructure of the metal surface itself; thus the reaction is structure insensitive. Although we study a different reaction, this model could be applicable to our Pt surfaces in Region II. In contrast to our observation in Region I, Carberry (13) reported increasing specific rate with crystallite size when studying C_2H_4 oxidation on Pt crystallites of 10–180 nm size on an Al_2O_3 support in ethylene-lean mixtures. A reason for this can be that small crystallites bind oxygen more strongly than larger crystallites (and polycrystalline surfaces) do (47). In addition, it cannot be excluded that the support itself took active part in some reaction step in Carberry's experiments. We are presently investigating the structure sensitivity of a similar system, Pt islands on SiO_2, and the results will be reported elsewhere (30).

Reaction Orders

In order to evaluate reaction orders, we fitted our entire collection of rate data to various functional expressions of the type

$$R \propto F_{C_2H_4}^{x} \cdot F_{O_2}^{y}. \qquad [4]$$

In Region I, a reasonable fit is found for $x = +1$ and $y = -1$, as illustrated in Fig. 8a. Thus the reaction is first order in C_2H_4, in line with data shown in Table 1, and negative first order in O_2. To our knowledge, reaction orders in O_2 have been previously reported only by Vayenas *et al.* (17, 19, 20) and Mandler *et al.* (18), who found zero order (at $T > 470$ K) and negative first order (at $T < 360$ K), respectively.

In Region II, the data can be fitted fairly well with $x = -2$ and $y = +3$ close to the rate maximum (Fig. 8b). A weaker dependence, $x = -0.5$ and $y = +1$(Fig. 8c), is found in large C_2H_4 excess. The inhibitory effect of C_2H_4 in fuel-rich mixtures is well-documented (Table 1), but our data definitely have a more complex pressure dependence than the simple models (order -1 or 0 in C_2H_4 (12–20) and $+1$ in O_2 (12, 15, 17–20)) suggested before. This may simply be due to the fact that the present study is extended much further into the fuel-rich pressure regime. Negative half order in C_2H_4 has also been found in C_2H_4 hydrogenation on Pt (46), suggesting similar rate-limiting mechanisms in large C_2H_4 excess.

We conclude that *mapping the kinetics of a reaction over a narrow pressure range near some equilibrium point (e.g., rate maximum) is not always sufficient to allow predictions of the kinetics far away from that point.*

Reaction Probabilities and Sticking Coefficients

Figures 9a and 9b show the reaction probabilities of O_2 and C_2H_4 on the film at 423 K. In the case of oxygen, it might be tempting to assume that the reaction probability (r_{O_2}) is always equal to the sticking coefficient (s_{O_2}), since standard TPD experiments in UHV have shown that oxygen atoms on Pt recombine and desorb only at $T > 600$ K, which corresponds to a heat of desorption of the order of 200 kJ/mol (48–53). However, O_2 exposures of low-index surfaces in UHV seldom give more than a coverage $\theta_O = 0.25$, i.e., one oxygen atom per four Pt atoms (49, 51, 53–58). It has been demonstrated that 'higher' O_2 pressures (10^{-5}–10^{-7} Torr; still far lower than the pressures in this study) produce coverages close to unity (58, 59). Similar results have also been found in chemisorption studies at near-atmospheric pressures (60). It has further been shown that the heat of desorption for near-monolayer coverage drops to about half the low-coverage value (61). Therefore, Fig. 9a may give an underestimate of s_{O_2} in Region I. For ethylene (Fig. 9b), molecular desorption is large under fuel-rich conditions (3, 5–7,

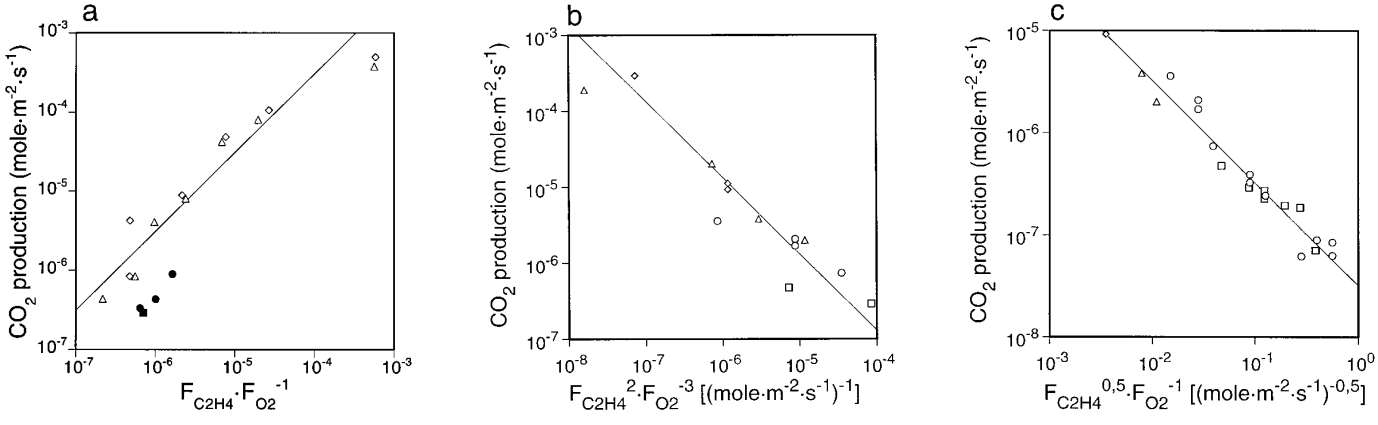

FIG. 8. Evaluation of reaction orders for a Pt film at $T = 423$ K. The measurements were performed at the O_2 pressures 0.30 Torr (□), 3.0 Torr (○), 150 Torr (△), and 1500 Torr (◇). The filled symbols indicate less accurate, "high-depletion" measurements (see Experimental Details). (a) CO_2 production rate vs $F_{C_2H_4}/F_{O_2}$ in Region I. (b) CO_2 production rate vs $F_{C_2H_4}^2/F_{O_2}^3$ in Region II, near the rate maximum. (c) CO_2 production rate vs $\sqrt{F_{C_2H_4}}/F_{O_2}$ in Region II, further away from the rate maximum.

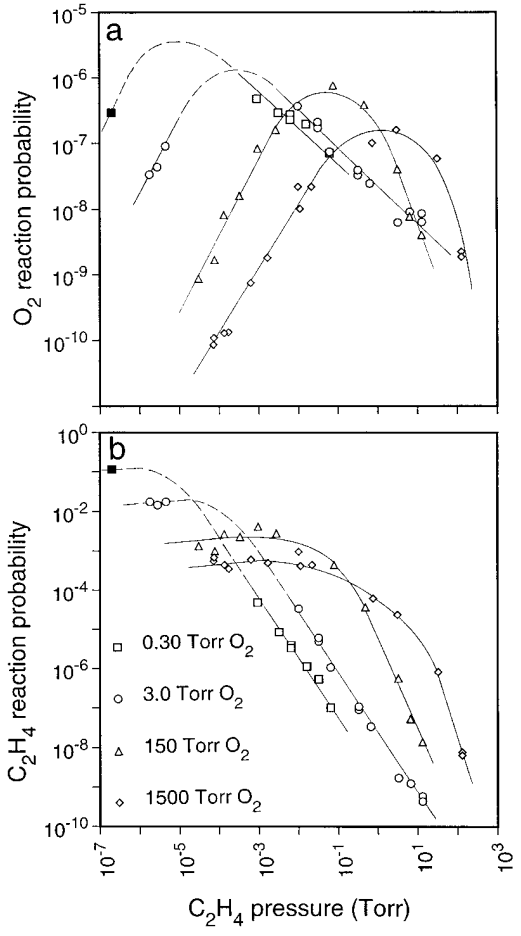

FIG. 9. (a) The O_2 reaction probability as a function of the C_2H_4 pressure. The symbols correspond to various constant O_2 pressures as defined in Fig. 9b. (b) The C_2H_4 reaction probability as a function of the C_2H_4 pressure. The sample was a Pt film at $T = 423$ K. The filled symbols indicate less accurate, "high-depletion" measurements (see Experimental Details). Lines are only drawn as a guide to the eye.

9, 10), and thus we expect the sticking coefficient ($s_{C_2H_4}$) to exceed the reaction probability ($r_{C_2H_4}$) in Region II.

At the higher O_2 pressures in Fig. 9a, r_{O_2} is very low compared with reported sticking coefficients on clean Pt (48, 49, 51, 53–55, 62), even at the rate maximum, which implies that there is a large, blocking coverage of surface species regardless of reactant mixture. At the lower O_2 pressures, r_{O_2} cannot be measured near the rate maximum due to the inherent instability discussed under 'Experimental Details'. At all O_2 pressures, however, r_{O_2} drops with increasing C_2H_4 pressure in Region II, indicating that adsorbed ethylene (or ethylene-derived intermediates) further increases the inhibition of O_2 adsorption.

Figure 9b shows that impinging C_2H_4 molecules react more easily than O_2 for almost all tested gas mixtures. At the lower O_2 pressures in Region I, $r_{C_2H_4}$ is high ($\geq 10^{-2}$, entering the region of extreme depletion, where the SRGS evaluation procedure gives poor accuracy (34)). In fact, it is only about one order of magnitude smaller than "initial" sticking coefficients in UHV (2), despite a large oxygen coverage. However, $r_{C_2H_4}$ drops below 10^{-3} at higher O_2 pressures, which shows that surface oxygen inhibits C_2H_4 adsorption.

There are similarities between Figs. 9a and 9b which may be explained by molecular desorption of excess reactants. It is observed that

(i) $r_{C_2H_4}$ is independent of C_2H_4 pressure in Region I, whereas

(ii) r_{O_2} is a function of both O_2 and C_2H_4 pressure in Region I.

Our interpretations are as follows:

(a) It is suggested by (i) that the surface is completely dominated by oxygen and that the coverage of ethylene-derived species is negligible.

(b) It follows from (a) that the sticking coefficient of oxygen should depend only on the O_2 pressure in Region I.

(c) Interpretation (b) appears to be in conflict with observation (ii), but it can be rationalized if *we postulate that molecular desorption of O_2 dominates over the oxidation reaction in large excess of oxygen*, in line with the discussion at the beginning of this section. Analogous arguments can be applied at the lower O_2 pressures in Region II, where r_{O_2} depends only on C_2H_4 pressure. Thus we believe that C_2H_4 desorption is dominant in large C_2H_4 excess.

It should also be observed that $r_{C_2H_4}$ does not remain constant with increasing C_2H_4 pressure all the way up to the rate maximum, at least not at the higher O_2 pressures. We interpret the point where $r_{C_2H_4}$ starts to decrease as the point where θ_O is no longer solely determined by the O_2 pressure, i.e., θ_O is no longer constant, and coverages of other species begin to build up on the surface.

C–V Signal

Figure 10 shows the C–V signal from a Pt film sample upon exposure to six C_2H_4 pulses in 1500-Torr O_2. The response time is extremely long compared with the mass spectrometer signals, which normally reach a steady state within a few seconds after a pressure change. Therefore, the speed of response must be controlled by processes other than the observed surface chemistry; hydrogen diffusion is possibly slow through our Pt films. While the slow response makes quantitative observations difficult, there are still qualitative conclusions to be drawn.

First, the C–V signal shows that free hydrogen is formed at the four highest C_2H_4 pressures, thus confirming that C_2H_4 dissociates on the Pt surface. Second, there is hardly any hydrogen response at the two lowest C_2H_4 pressures. This indicates, we believe, that the surface is completely dominated by oxygen in Region I, as suggested in the previous section. Third, the C–V signal has a "breakthrough"

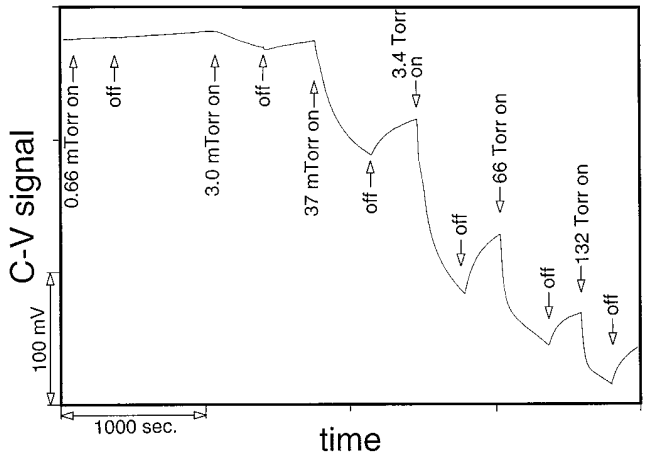

FIG. 10. C–V signal from a Pt film exposed to six C_2H_4 pulses at $T = 423$ K. A negative shift in the C–V signal corresponds to an increase of the hydrogen coverage on the Pt surface. The O_2 pressure was 1500 Torr and the nominal C_2H_4 pressures was 6.3 mTorr, 63 mTorr, 0.63 Torr, 6.6 Torr, 66 Torr, and 132 Torr. The true surface pressures, as evaluated by SRGS, are indicated in the figure.

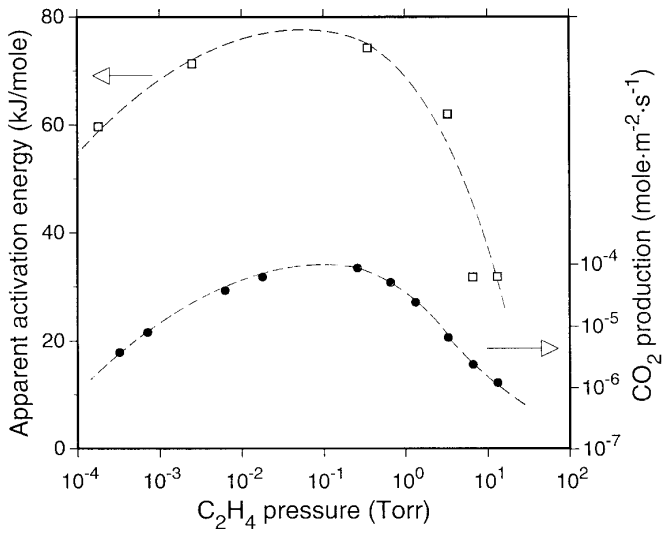

FIG. 11. Apparent activation energy vs C_2H_4 pressure for a Pt film at 150 Torr O_2, calculated from rate measurements at $T = 373$–423 K. The CO_2 production rate at $T = 398$ K is also shown. Lines are drawn only as a guide to the eye.

in a rather narrow C_2H_4 pressure region (at $\approx 10^{-2}$ Torr in Fig. 10). This occurs at a C_2H_4 pressure far lower than the pressure needed for maximum reaction rate (see Fig. 6), and it coincides well with the point where the C_2H_4 reaction probability starts to decrease (see Fig. 9b). Thus it seems that the constant C_2H_4 reaction probability and the lack of hydrogen response at low C_2H_4 pressures have a common explanation: the oxygen coverage is near saturation.

Apparent Activation Energy

The temperature dependence of the reaction was also investigated. Rates were measured at 150 Torr O_2 and $T = 373$–423 K and fitted to the standard Arrhenius expression. The resulting *apparent* activation energies (E^a), calculated for six different C_2H_4 pressures, are given in Fig. 11. Values of 30–75 kJ/mol are found and the maximum energy coincides with the rate maximum. Literature data on E^a (Table 1) scatter considerably, and this is not surprising in view of the various experimental conditions. Cant and Hall (12) and Hawkins and Wanke (15) obtained 77 and 102 kJ/mol, respectively, in ethylene excess and at temperatures and pressures similar to ours. Other groups (16, 17, 19) have observed significantly different values of E^a on either side of the rate maximum, in contrast to the quite symmetric curve in Fig. 11, despite the limited range of pressures in their experiments. It should be emphasized again, however, that there is a lack of comparable data for dense, macroscopic Pt surfaces; E^a has been determined only in an early work by Patterson and Kemball (11), who found 49 kJ/mol under fuel-rich conditions, well within the limits of our measurements.

In conclusion, the various values of E^a in Table 1 and in Fig. 11 confirm that *apparent activation energies (as well as reaction orders) may depend strongly on the experimental conditions and thus they cannot always be accepted as "universal parameters."*

A Qualitative Model

It is beyond our intentions to work out a detailed, quantitative kinetic model of ethylene oxidation on Pt, since that would require additional (spectroscopic) information on the nature of surface intermediates and their coverage dependence. Nevertheless, we will propose a very simple reaction scheme, which seems to fit the qualitative features of our rate data under excess conditions of either reactant.

In accordance with previous studies (16, 18, 21, 26, 27), we assume a L–H mechanism; i.e., both reactants must adsorb before reacting:

$$O_2(g) \leftrightarrow 2O(a) \qquad [5]$$

$$C_2H_4(g) \leftrightarrow C_2H_4(a). \qquad [6]$$

The surface reaction is probably composed of several elementary steps, involving various reaction intermediates. For simplicity, we lump them together into a direct reaction between the adsorbed reactants:

$$C_2H_4(a) + 6O(a) \rightarrow 2CO_2(g) + 2H_2O(g). \qquad [7]$$

The sticking coefficient of O_2 is assumed to follow a second-

order expression (51, 53, 62),

$$s_{O_2} = s^i_{O_2}\chi^2, \quad [8]$$

where $s^i_{O_2}$ is a coverage-independent factor (often called "initial sticking coefficient") and χ is a coverage-dependent "inhibition factor" (often set equal to the fraction of unoccupied surface sites). We further assume that this inhibition factor governs the sticking coefficient of C_2H_4 in a similar way,

$$s_{C_2H_4} = s^i_{C_2H_4}\chi^\alpha, \quad [9]$$

where different values may be assigned to the exponent α in Region I and Region II, respectively. The reaction steps [5]–[7] give steady-state balance equations for adsorbed oxygen and ethylene,

$$2s_{O_2}F_{O_2} - 2d_{O_2}\theta_O^2 - 3R_{CO_2} = 0 \quad [10]$$

$$s_{C_2H_4}F_{C_2H_4} - d_{C_2H_4}\theta_{C_2H_4} - \tfrac{1}{2}R_{CO_2} = 0, \quad [11]$$

respectively, where R_{CO_2} is the formation rate of CO_2, F_i are impingement rates, and d_i are rate constants of desorption.

In ethylene excess, we assume that C_2H_4 desorption is abundant and O_2 desorption is negligible; i.e., $d_{O_2}\theta_O^2 \ll R_{CO_2} \ll d_{C_2H_4}\theta_{C_2H_4}$. Equations [8]–[11] then yield

$$R_{CO_2} = \tfrac{2}{3}s^i_{O_2}F_{O_2}\left(\frac{d_{C_2H_4}\theta_{C_2H_4}}{s^i_{C_2H_4}F_{C_2H_4}}\right)^{\frac{2}{\alpha}} \quad \text{(ethylene excess)}. \quad [12]$$

As mentioned previously, we expect $\theta_{C_2H_4}$ to be close to saturation and, therefore, nearly pressure-independent. The impingement rates are proportional to pressures (Eq. [2]) and, consequently, Eq. [12] gives a reaction order of +1 in O_2 and $-(2/\alpha)$ in C_2H_4. Thus the experimental reaction orders (+1 and −0.5) are obtained if we choose $\alpha = 4$. This large value of α implies that C_2H_4 adsorption is a strongly self-inhibiting process. A similar fourth power dependence between $s_{C_2H_4}$ and the fraction of unoccupied surface has been reported previously by Fischer and Kelemen (2) and Windham *et al.* (4).

In oxygen excess, reverse conditions are assumed, i.e., O_2 desorption is dominant. The reaction rate then becomes

$$R_{CO_2} = 2s^i_{C_2H_4}F_{C_2H_4}\left(\frac{d_{O_2}\theta_O^2}{s^i_{O_2}F_{O_2}}\right)^{\frac{\alpha}{2}} \quad \text{(oxygen excess)}. \quad [13]$$

Again, we assume that the coverage of the excess reactant has a negligible pressure dependence. Equation [13] then gives reaction orders identical with the empirical values (−1 in O_2 and +1 in C_2H_4), provided that we choose $\alpha = 2$. To our knowledge, the coverage dependence of $s_{C_2H_4}$ on Pt surfaces precovered with oxygen is not known in detail. However, it has been shown that C_2H_4 may adsorb even in presence of high oxygen coverages (8–10); thus it is not unreasonable that α is smaller in oxygen excess than in ethylene excess.

There are a few comments to be made concerning this model. It is well-known (and also confirmed by our C–V measurements) that C_2H_4 dissociates to some extent upon adsorption on Pt above room temperature (1–10), even in absence of oxygen. The dissociation and the reaction with oxygen is likely to produce a variety of coexisting intermediates on the surface. However, the sticking coefficients, Eqs. [8]–[9], contain no explicit dependence on coverages of various surface species; it is only assumed that the inhibition factor χ is the same for both reactants. Extensive studies by Somorjai and co-workers (1, 46) have indicated that ethylene exposure produces a rather stable carbonaceous overlayer on Pt and that hydrocarbon conversion reactions may proceed on top of this overlayer. Such an overlayer is probably built up on our samples in ethylene excess. Therefore, $s^i_{O_2}$ and $s^i_{C_2H_4}$ should be interpreted only as coverage-independent factors in Eq. [12], and not as sticking coefficients of a clean surface. Furthermore, it is not necessary that the desorption of C_2H_4 and O_2 follow the kinetics indicated in Eqs. [10]–[11]; the only prerequisite is that desorption of the excess reactant is dominant and near saturation.

It is interesting to compare the temperature dependences of Eqs. [12]–[13] with the apparent activation energies shown in Fig. 11. Impingement rates depend weakly on T (see Eq. [2]). Assuming that this is the case also for $s^i_{O_2}$ and $s^i_{C_2H_4}$, most of the T-dependence in Eqs. [12]–[13] must be hidden in the desorption constants. Desorption constants are usually of the Arrhenius form; i.e.,

$$d_i \propto \exp\left(-\frac{E^d_i}{RT}\right). \quad [14]$$

Thus, it is easily found from Eq. [13] that

$$E^d_{O_2} \approx E^a_I \quad [15]$$

and, from Eq. [12],

$$E^d_{C_2H_4} \approx 2E^a_{II}, \quad [16]$$

where $E^d_{O_2}$ and $E^d_{C_2H_4}$ are desorption energies and E^a_I and E^a_{II} are apparent activation energies in Regions I and II, respectively. Using the extreme values of Fig. 11, $E^a_I = 60$ kJ/mol and $E^a_{II} = 30$ kJ/mol, we get $E^d_{O_2} \approx 60$ kJ/mol and $E^d_{C_2H_4} \approx 60$ kJ/mol. The former is lower than the 117 kJ/mol O_2 desorption energy for $\theta_O = 0.75$ on Pt (111) reported by Parker *et al.* (61); however, our oxygen coverage may possibly be higher than 0.75. Our value of $E^d_{C_2H_4}$ is well within the range of available literature data (30–75 kJ/mol) (3, 5, 6, 10). The latter comparison is somewhat questionable, since C_2H_4 desorption energies are usually determined from TPD peaks below the C_2H_4 dissociation temperature. We are not

aware of any experiments of C_2H_4 desorption from Pt surfaces covered with carbonaceous fragments. It is evident that more experimental data on C_2H_4 and O_2 desorption rates from Pt surfaces at high pressures (e.g., by isotope exchange experiments) would be needed for further tests of this model.

CONCLUSIONS

This paper demonstrates the power of a the new SRGS method for reaction studies far into the viscous pressure regime. The reaction between C_2H_4 and O_2 on polycrystalline Pt surfaces was characterized over a pressure range of unique extent (eight and four orders of magnitude in C_2H_4 and O_2, respectively) and at temperatures between 373 and 473 K. CO_2 and H_2O were the only detected reaction products. Structure insensitivity was observed at all reactant mixtures for grain sizes between 10 and 1000 nm. C_2H_4 was found to have a much higher reaction probability than O_2, leading to a reaction rate maximum at a C_2H_4/O_2 ratio of 10^{-4}–10^{-3}, i.e., far below a stoichiometric reactant mixture. An asymptotic rate behavior with fairly constant reaction orders in C_2H_4 and O_2 was found on either side of the rate maximum, but it was necessary to change the C_2H_4/O_2 ratio by at least two orders of magnitude from the rate maximum to reach into these asymptotic regions. The reaction orders in oxygen excess were $+1$ in C_2H_4 and -1 in O_2, while -0.5 in C_2H_4 and $+1$ in O_2 were found in large ethylene excess. In weak ethylene excess, a stronger dependence was observed (order ≈ -2 in C_2H_4 and $\approx +3$ in O_2). The maximum apparent activation energy, determined at an O_2 pressure of 150 Torr, was about 75 kJ/mol and it coincided with the rate maximum. On either side of the rate maximum, the activation energy was found to decrease. Hydrogen detection by the C–V technique clearly indicated a release of hydrogen atoms on the surface upon C_2H_4 adsorption. The observed reaction orders and activation energies could be qualitatively fitted to a simple L–H reaction scheme, assuming that (i) adsorption of C_2H_4 and O_2 is competitive, (ii) molecular reactant desorption is faster than the reaction in the excess regimes, (iii) surface coverages are near saturation, and (iv) the inhibition of C_2H_4 adsorption is moderate (second order) in oxygen excess and strong (fourth order) in ethylene excess.

ACKNOWLEDGMENTS

We thank Mr. M. Eriksson for useful comments on the manuscript. This work has been supported by grants from the Swedish Natural Science Research Council (NFR), the Swedish National Board for Industrial and Technical Development (NUTEK), and the Swedish Research Council for Engineering Sciences (TFR).

REFERENCES

1. Somorjai, G. A., "Introduction to Surface Chemistry and Catalysis." Wiley, New York, 1994 [and references therein].
2. Fischer, T. E., and Kelemen, S. R., *Surf. Sci.* **69**, 485 (1977).
3. Salmerón, M., and Somorjai, G. A., *J. Phys. Chem.* **86**, 341 (1982).
4. Windham, R. G., Koel, B. E., and Paffett, M. T., *Langmuir* **4**, 1113 (1988).
5. Windham, R. G., Bartram, M. E., and Koel, B. E., *J. Phys. Chem.* **92**, 2862 (1988).
6. Mohsin, S. B., Trenary, M., and Robota, H. J., *Chem. Phys. Lett.* **154**, 511 (1989).
7. Pettiette-Hall, C. L., Land, D. P., McIver, R. T., Jr., and Hemminger, J. C., *J. Phys. Chem.* **94**, 1948 (1990).
8. Palmer, R. L., *J. Vac. Sci. Technol.* **12**, 1403 (1975).
9. Steininger, H., Ibach, H., and Lehwald, S., *Surf. Sci.* **117**, 685 (1982).
10. Berlowitz, P., Megiris, C., Butt, J. B., and Kung, H. H., *Langmuir* **1**, 206 (1985).
11. Patterson, W. R., and Kemball, C., *J. Catal.* **2**, 465 (1963).
12. Cant, N. W., and Hall, W. K., *J. Catal.* **16**, 220 (1970).
13. Carberry, J. J., *Kinet. Katal.* **18**, 562 (1977).
14. Carberry, J. J., *Acc. Chem. Res.* **18**, 358 (1985).
15. Hawkins, J. R., and Wanke, S. E., *Can. J. Chem. Eng.* **57**, 621 (1979).
16. Paspek, S. C., and Varma, A., *Chem. Eng. Sci.* **35**, 33 (1980).
17. Vayenas, C. G., Lee, B., and Michaels, J., *J. Catal.* **66**, 36 (1980).
18. Mandler, J., Lavie, R., and Sheintuch, M., *Chem. Eng. Sci.* **38**, 979 (1983).
19. Bebelis, S., and Vayenas, C. G., *J. Catal.* **118**, 125 (1989).
20. Vayenas, C. G., Bebelis, S., and Despotopoulou, M., *J. Catal.* **128**, 415 (1991).
21. Sant, R., Kaul, D. J., and Wolf, E. E., *AIChE J.* **35**, 267 (1989).
22. Kaul, D. J., and Wolf, E. E., *Chem. Eng. Sci.* **41**, 1101 (1986).
23. Onken, H. U., and Wolf, E. E., *Chem. Eng. Sci.* **43**, 2251 (1988).
24. Onken, H. U., and Wolf, E. E., *Chem. Eng. Sci.* **47**, 1659 (1992).
25. Vayenas, C. G., Georgakis, C., Michaels, J., and Tormo, J., *J. Catal.* **67**, 348 (1981).
26. Sheintuch, M., and Avichai, M., *Ind. Eng. Chem. Res.* **27**, 1152 (1988).
27. Sheintuch, M., Schmidt, J., and Rosenberg, S., *Ind. Eng. Chem. Res.* **28**, 955 (1989).
28. Kunimori, K., Iwade, T., and Uetsuka, H., *J. Electr. Spec. Rel. Phenom.* **64/65**, 451 (1993).
29. Wu, N. L., and Phillips, J., *J. Catal.* **113**, 383 (1988).
30. Ackelid, U., Wallenberg, L. R., and Petersson, L.-G., *Catal. Lett.,* in press.
31. Ackelid, U., Fogelberg, J., and Petersson, L.-G., *Vacuum* **42**, 889 (1991).
32. Petersson, L.-G., and Ackelid, U., *Surf. Sci.* **269/270**, 500 (1992).
33. Lundgren, S., Keck, K.-E., and Kasemo, B., *Rev. Sci. Instrum.* **65**, 2696 (1994).
34. Ackelid, U., "Linköping Studies in Science and Technology," dissertation 393, Linköping University, Linköping, Sweden, 1995.
35. Lundström, I., Armgarth, M., and Petersson, L.-G., *CRC Crit. Rev. Solid State Mater. Sci.* **15**, 201 (1989) [and references therein].
36. Spetz, A., Helmersson, U., Enquist, F., Armgarth, M., and Lundström, I., *Thin Solid Films* **177**, 77 (1989).
37. Niehus, H., and Comsa, G., *Surf. Sci.* **102**, L14 (1981).
38. Bonzel, H. P., Franken, A. M., and Pirug, G., *Surf. Sci.* **104**, 625 (1981).
39. Mundschau, M., and Vanselow, R., *Surf. Sci.* **157**, 87 (1985).
40. Akhter, S., Greenlief, C. M., Chen, H.-W., and White, J. M., *Appl. Surf. Sci.* **25**, 154 (1986).
41. Kasemo, B., *Rev. Sci. Instr.* **50**, 1602 (1979).
42. Sze, S. M., "Physics of Semiconductor Devices." Wiley, New York, 1981.
43. Smith, J. M., "Chemical Engineering Kinetics." McGraw–Hill, New York, 1981.
44. Satterfield, C. N., "Mass Transfer in Heterogeneous Catalysis." MIT Press, London, 1970.
45. Beusch, H., Fieguth, P., and Wicke, E., *Chem. Ing. Tech.* **44**, 445 (1972).
46. Zaera, F., and Somorjai, G. A., *J. Am. Chem. Soc.* **106**, 2288 (1984).
47. McCabe, R. W., Wong, C., and Woo, H. S., *J. Catal.* **114**, 354 (1988).

48. Schwaha, K., and Bechtold, E., *Surf. Sci.* **65**, 277 (1977).
49. Gland, J. L., and Korchak, V. N., *Surf. Sci.* **75**, 733 (1978).
50. Barteau, M. A., Ko, E. I., and Madix, R. J., *Surf. Sci.* **102**, 99 (1981).
51. Campbell, C. T., Ertl, G., Kuipers, H., and Segner, J., *Surf. Sci.* **107**, 220 (1981).
52. McClellan, M. R., McFeely, F. R., and Gland, J. L., *Surf. Sci.* **123**, 188 (1983).
53. Winkler, A., Guo, X., Siddiqui, H. R., Hagans, P. L., and Yates, J. T., Jr., *Surf. Sci.* **201**, 419 (1988).
54. Monroe, D. R., and Merill, R. P., *J. Catal.* **65**, 461 (1980).
55. Gland, J. L., *Surf. Sci.* **93**, 487 (1980).
56. Steininger, H., Lehwald, S., and Ibach, H., *Surf. Sci.* **123**, 1 (1982).
57. Cudok, A., Froitzheim, H., and Hess, G., *Surf. Sci.* **307–309**, 761 (1994).
58. Derry, G. N., and Ross, P. N., *Surf. Sci.* **140**, 165 (1984).
59. Neuhaus, D., Joo, F., and Feuerbacher, B., *Phys. Rev. Lett.* **58**, 694 (1987).
60. O'Rear, D. J., Löffler, D. G., and Boudart, M., *J. Catal.* **121**, 131 (1990). [and references therein]
61. Parker, D. H., Bartram, M. E., and Koel, B. E., *Surf. Sci.* **217**, 489 (1989).
62. Ljungström, S., Kasemo, B., Rosén, A., Wahnström, T., and Fridell, E., *Surf. Sci.* **216**, 63 (1989).